Adsorption of Pb(II) by UV-aged microplastics and cotransport in homogeneous and heterogeneous porous media

Journal of Hazardous Materials

Chang, Bokun; Huang, Zixuan; Yang, Xiaodong; Yang, Tianhuan; Fang, Xianhui et al

https://doi.org/10.1016/j.jhazmat.2023.133413

Journal of Hazardous Materials 465 (2024) 133413

Contents lists available at ScienceDirect

Journal of Hazardous Materials

journal homepage: www.elsevier.com/locate/jhazmat

Adsorption of Pb(II) by UV-aged microplastics and cotransport in homogeneous and heterogeneous porous media

Bokun Chang [a], Zixuan Huang [a], Xiaodong Yang [a], Tianhuan Yang [a], Xianhui Fang [a], Xianbao Zhong [a], Wei Ding [a], Gang Cao [a,b], Yajun Yang [a], Feinan Hu [a,c], Chenyang Xu [a], Ling Qiu [d], Jialong Lv [a,e,*], Wei Du [a,e,*]

[a] College of Natural Resources and Environment, Northwest A&F University, Yangling 712100, China
[b] Soil Physics and Land Management Group, Wageningen University & Research, 6708 PB Wageningen, the Netherlands
[c] Institute of Soil and Water Conservation, Chinese Academy of Sciences and Ministry of Water Resources, Yangling 712100, China
[d] College of Mechanical and Electronic Engineering & Northwest Research Center of Rural Renewable Energy, Exploitation and Utilization of Ministry of Agriculture, Northwest A&F University, Yangling 712100, China
[e] Key Laboratory of Plant Nutrition and the Agro-environment in Northwest China, Ministry of Agriculture, Yangling 712100, China

HIGHLIGHTS

- UV irradiation increases surface electronegativity and specific surface area of MPs.
- Oxygen-containing functional groups dominate the adsorption of Pb(II) by aged MPs.
- Greater inherent mobility of aged MPs could carry more Pb(II) for co-transport.
- Intricate pore structure of biochar prevents both contaminants from diffusing.

GRAPHICAL ABSTRACT

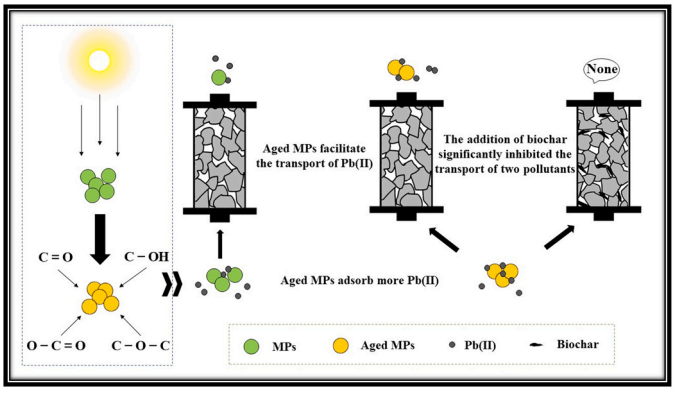

ARTICLE INFO

Editor: Meiping Tong

Keywords:
Plastic particles
UV aging
Lead ions
Oxygen functional group
Passivation of contaminants
DLVO theory
Two-point adsorption kinetics

ABSTRACT

To investigate the adsorption effects of aged microplastics (MPs) on Pb(II) and their co-transport properties in homogeneous (quartz sand) and heterogeneous (quartz sand with apple branches biochar) porous media, we explored the co-transport of UV-irradiated aged MPs and coexisting Pb(II) along with their interaction mechanisms. The UV aging process increased the binding sites and electronegativity of the aged MPs' surface, enhancing its adsorption capacity for Pb(II). Aged MPs significantly improved Pb(II) transport through homogeneous media, while Pb(II) hindered the transport of aged MPs by reducing electrostatic repulsion between these particles and the quartz sand. When biochar, with its loose and porous structure, was used as a porous medium, it effectively inhibited the transport capacity of both contaminants. In addition, since the aged MPs cannot penetrate the column, a portion of Pb(II) adsorbed by the aged MPs will be co-deposited with the aged

* Corresponding authors at: College of Natural Resources and Environment, Northwest A&F University, Yangling 712100, China.
E-mail addresses: ljlll@nwsuaf.edu.cn (J. Lv), weidu@nwafu.edu.cn (W. Du).

https://doi.org/10.1016/j.jhazmat.2023.133413
Received 23 October 2023; Received in revised form 20 December 2023; Accepted 29 December 2023
Available online 2 January 2024

MPs, hindering Pb(II) transport to a greater extent. The transport experiments were simulated and interpreted using two-point kinetic modeling and the DLVO theory. The study results elucidate disparities in the capacity of MPs and aged MPs to transport Pb(II), underscoring the potential of biochar application as an effective strategy to impede the dispersion of composite environmental pollutants.

1. Introduction

The degradation of larger plastic products, industrial processes, and everyday consumer items such as personal care products and textiles [2,69,72,75], resulting in the release of microplastics (MPs) into the environment, has grown in importance as a concern for the environment recently [31,32]. These particles can be consumed by a wide variety of organisms, spanning from plankton and fish to birds and mammals, resulting in adverse health and behavioral effects [35,49]. MPs' distinct surface properties, such as size, porosity, specific surface area, and hydrophobicity, facilitate the adsorption and accumulation of various contaminants and make them excellent carriers [12,31,7]. As a result, more of the hazardous substances spread by MPs will be reintroduced into the environment as the MPs degrade and pose a potential threat to ecosystems [12,3,55]. MPs, in particular, have the potential to interact with other environmental contaminants, altering their toxicity and bioavailability, and ultimately influencing the ecological security of the region by controlling the transport of other pollutants [45,72]. Among the common environmental contaminants, heavy metals are of particular concern due to their persistence, bioaccumulation, and toxic effects even at low exposure levels [5]. Lead ions can persist in the environment and accumulate in soil, water, and the food chain [10,11]. Notably, lead ions have been observed to have a higher affinity for various colloids in soil water compared to other heavy metal ions such as copper and cadmium ions [10,14,68]. Although the strong interactions between lead ions and MPs have been documented by batch adsorption and column transport investigations [26,70], the cotransport of them in various porous media is still insufficient. Therefore, investigating the interaction mechanisms between MPs and lead ions and understanding their environmental transport behavior is crucial for developing effective management strategies to mitigate their adverse effects on the environment and human health [61,68].

The interaction between MPs and lead ions occurs primarily through the process of adsorption, whereby lead ions adhere to the surface of MPs [68]. Several factors could influence this process, including the surface charge and functional groups of the MPs, as well as the pH and ionic strength of the surrounding water [46,53,59]. The surface of MPs has been found to act as a reservoir for heavy metals, thereby facilitating their spatial transport [72,73]. Furthermore, heavy metal ions can induce changes in the hydrated particle size and surface charge of MPs colloids through ion-MPs surface complexation [59]. These changes in physicochemical properties can affect the stability and mobility of MPs during the transport process. Polystyrene, a commonly used model material for studying MPs transport in saturated porous media, exhibits properties similar to those of other types of MPs, such as low density, high stability, and resistance to degradation [28]. While pristine polystyrene is commonly used to model the transport of MPs in saturated porous media, it is crucial to consider the influence of natural environmental factors on the transport of MPs, such as aging caused by ultraviolet (UV) radiation [51]. UV light generates oxygen-containing functional groups on the surface of aged MPs, causing them to become more polar, porous, hydrophilic, and charged [51]. These changes in the physicochemical properties of aged MPs can significantly affect the interaction between aged MPs and lead ions [48], which ultimately influences the sorption, transport, and retention behavior of lead ions as aged MPs present [70].

While it is important to continue researching the interaction mechanisms between MPs and heavy metals in various habitats, it is equally crucial to emphasize the significance of investigating their diffusion inhibition in the environment [30,47]. Biochar, a carbonaceous material derived from the pyrolysis of organic matter, has emerged as a promising tool in environmental science [60,63]. Its highly porous structure and extensive surface area make it an efficient adsorbent for various pollutants [29]. In the realm of soil remediation, biochar is widely recognized as an effective adsorbent that reduces the mobility of soil contaminants, thereby minimizing the risk of groundwater and surface water contamination [20,67]. The plentiful functional groups in biochar offer abundant binding sites for heavy metals to form complexes, while the mineral elements in biochar promote heavy metal adsorption through precipitation, resulting in the formation of metal oxides, chlorides, sulfates, or other precipitates [40]. Moreover, existing studies have indicated that filling sand columns with biochar can effectively inhibit the transport of MPs [23,62]. Tong et al. [62] found that biochar/Fe_3O_4-biochar, when thoroughly mixed with quartz sand, significantly retained MPs with diameters of 0.02 μm and 2 μm in sand columns. Hsieh et al. [23] showed that woodchip-extracted biochar achieved complete removal of MPs in real river and sewage samples. Significant progress has been made in understanding the impact of using biochar as a porous medium on the standalone transport of MPs. However, uncertainties persist regarding whether these insights can adequately elucidate the mechanisms involved in the co-transport of both MPs and lead ions.

This study has three specific goals. First, investigate the influence of UV irradiation on the surface physical and chemical properties of MPs. Second, elucidate the interaction mechanisms and cotransport behavior of aged MPs and Pb(II) in saturated porous media. Finally, investigate the effect of biochar incorporation into quartz sand on the transport of these two coexisting contaminants. The results of this study have important implications for the management and remediation of MPs and heavy metal contamination in natural systems.

2. Materials and methods

2.1. Materials

In this study, $Pb(NO_3)_2$ was purchased from Shanghai Aladdin Bio-Chem Technology Co., Ltd. Monodisperse green fluorescent polystyrene particles (500 nm in diameter and 1.05 g/cm^3 in density) obtained from Tianjin Best Chromatography Technology Development Center were used as model MPs. UV aging experiments were conducted to simulate the natural UV exposure of MPs in aquatic environments using a chamber equipped with four UVA-340 lamps, each with a power rating of 8 watts. Specifically, to obtain aged MPs suspension, a beaker containing 200 mg/L MPs suspension was placed inside the aging chamber for one month, and the suspension was kept hydrated by daily water replenishment and ultrasonic dispersion [58].

High-purity quartz sand (Qinfeng quartz factory in Zhouzhi County, Shaanxi Province, China), with particle sizes ranging from 0.4 mm to 0.6 mm, was used as the porous medium for filling Plexiglas columns. The quartz sand was sequentially washed with tap water, 0.1 M HCl, and 0.1 M NaCl to remove impurities and metal oxides from its surface [6]. The sand was then rinsed several times with deionized water until the pH value of the filtrate approached neutral, then dried at 105 ℃ and stored for future use.

The apple branches were selected as the raw material for biochar production in this study for the following reasons: Apple branch is an agricultural waste product, and utilizing such biomass for biochar production aligns with sustainability goals by repurposing waste materials

[38]. With low ash and moisture content and high lignin content, they are conducive to obtaining high-quality biochar [66], and serve as an ideal feedstock for biomass carbonization. The discarded apple branches were collected from the Baishui Apple Experimental Station of Northwest A&F University. The apple twigs were dried, crushed, and subsequently sifted through a 1 mm sieve. The resulting material was subjected to heating under N_2 protection at 550 ℃ for 2 h to obtain apple twig biochar. In the realm of soil remediation, biochar stands out as a potent adsorbent, curbing the mobility of soil contaminants and thereby mitigating the potential hazards of groundwater and surface water pollution [57]. Following precedent studies, a 0.5% mass ratio of biochar was meticulously blended with quartz sand [62]. This mixture was stored in a sealed container and used as a porous medium for conducting column transport experiments. A detailed characterization of the above-mentioned materials can be found in Supplementary Material S1.

2.2. Batch adsorption experiments

Batch adsorption experiments were conducted to evaluate the adsorption and desorption capacity of MPs and aged MPs for Pb(II). The experimental operation consisted of configuring 50 ml of different concentrations of Pb(II) mixed with 0.2 mg/L of MPs or aged MPs in a 100-ml centrifuge tube. To avoid hydrolysis of Pb(II), the pH value was set to 5.8 for all experiments according to the degree of hydrolysis of Pb (II) in different pH environments (Fig. S1) [39]. Subsequently, the mixtures were shaken in a constant-temperature shaking incubator until adsorption equilibrium was reached. The MPs/aged MPs were then separated from the solution by filtration, and the residual concentration of Pb(II) in the solution was measured using a flame spectrophotometer (AA530, PerkinElmer, USA). All experiments were performed in triplicate to ensure accuracy and reproducibility. The experiments were conducted under different conditions, including initial Pb(II) concentrations ranging from 10 to 50 mg/L, temperatures ranging from 25 to 45 °C, adsorption times ranging from 1 min to 4 h, and competing ion (Na^+) concentrations ranging from 0 to 20 mg/L. For more information on the batch adsorption experiments, see Supplementary Material S2.

2.3. Aggregation and sedimentation experiments

A suspension of MPs/aged MPs at a concentration of 20 mg/L or a suspension of MPs-Pb(II)/aged MPs-Pb(II) at a concentration of 20 mg/L for both MPs and Pb(II) was prepared and sonicated to ensure stable dispersion. The pH of both the suspension and electrolyte solution was adjusted to 5.8 using HCl and NaOH solutions, ensuring stability post-mixing. Subsequently, 1.8 ml of the suspension was mixed with an equal volume of electrolyte solution of varying concentrations, resulting in a final suspension with concentrations of 10 mg/L for both MPs and Pb(II). The aggregation kinetics curves of MPs and aged MPs were measured using a dynamic light scattering instrument (Brookhaven, Omni, USA) with an incident wavelength of 635 nm and a scattering angle of 90°. The sedimentation kinetic cuives of MPs and aged MPs were measured using a fluorescence spectrophotometer (97PRO, Prism, China) [7].

2.4. Column transport experiments

Column transport experiments were conducted to investigate the vertical transport behavior of MPs, aged MPs, and Pb(II) in a saturated porous medium. The wet packing method was used to fill a 15-cm-long, 3-cm-inner diameter organic glass column with either quartz sand or quartz sand with biochar. The column had a pore volume (PV) of approximately 45 ml and an average porosity (the ratio of the pore volume of the sand column to the total volume) of approximately 0.42. A 50-μm nylon mesh was placed at the top and bottom of the column to support the porous medium. To determine solute mobility and column performance, a non-reactive tracer experiment was performed using a potassium nitrate solution, and the convective dispersion coefficient was determined by fitting with Hydrus-1D. The column transport experiment involved the separate transport and co-transport of MPs/aged MPs and Pb(II) in the sand column under a background ion concentration (Na^+) of 1, 10, and 20 mM and a pH of 5.8 in the aqueous environment. Previous studies on the transport of MPs in saturated porous media used MPs concentrations ranging from 4 mg/L to 30 mg/L [36,37]. In our study, the MPs concentration was set at 10 mg/L, aligning with reported environmental ranges. This choice strikes a balance between realism and controlled experimentation [33,76]. To investigate the co-transport behavior of Pb(II) and MPs, the MPs needed to adsorb a certain amount of Pb(II). Therefore, Pb(II) was diluted to the required concentration of 10 mg/L under the experimental conditions, which was higher than the concentration found in natural waters [27]. Prior to the experiment, at least 10 PV of deionized water was pumped from the bottom to the top of the column using a peristaltic pump to remove air bubbles. A minimum of 3 PV of background electrolyte was then pumped into the column to stabilize the chemical composition of the solution. During the experiment, 3 PV of the target solution or target suspension with the same background electrolyte concentration was injected into the column. To ensure suspension stability, the suspension was sonicated for 10 min prior to injection. Subsequently, 3 PV of background electrolyte was pumped into the column to maintain the flow and ensure consistent conditions. The flow rate was set at 1 ml/min, and the effluent was collected continuously at 10-min intervals using a four-channel semi-automated collector. The concentrations of MPs/aged MPs and Pb(II) in the effluent were measured by fluorescence spectrophotometry and flame atomic absorption spectroscopy (AA530, PerkinElmer, USA), respectively. For details on the determination method of Pb(II) concentration during cotransport, see Supplementary Material S3. Breakthrough curves were obtained by monitoring the concentration changes of MPs/aged MPs and Pb(II) during their transport. Each treatment was replicated twice.

2.5. Mathematical model

In this study, the transport of MPs, aged MPs, and Pb(II) through saturated porous media was simulated using a two-site kinetic model based on the one-dimensional form of the convection-dispersion equation [4,52,58]. Further details regarding the methodology can be found in Supplementary Material S4.

The interactions between the MPs and the porous media were quantitatively characterized by the Derjaguin-Landau-Verwey-Overbeek (DLVO) theory, where the DLVO energy (V_{TOT}) is composed of van der Waals attraction (V_{VDW}) and electric double layer repulsion (V_{EDL}) [13,21,64]. Further details are given in Supplementary Material S5.

3. Results and discussion

3.1. Characterization of MPs/aged MPs

SEM-mapped images (Fig. 1) clearly reveal that the MPs exhibit a smooth, spherical shape, whereas the aged MPs display a rougher surface with visible cracks. Furthermore, there was no presence of oxygen elements observed on the surface of the MPs; however, a prominent distribution of oxygen elements could be distinctly observed on the surface of the aged MPs. The BET surface area analyzer was used to determine the specific surface area and mesopore volume of MPs and aged MPs, which found that the specific surface areas of MPs and aged MPs were 1.3982 m^2/g and 5.2378 m^2/g, respectively, and the mesopore volumes were 0.3212 cm^3/g and 0.7515 cm^3/g, respectively. XRD analysis revealed an increased crystallinity in aged MPs, indicating greater fragility and the formation of smaller particles (Fig. S2). However, it should be noted that UV irradiation is a slow aging process, and after 30 days of aging, there was no significant change in particle size

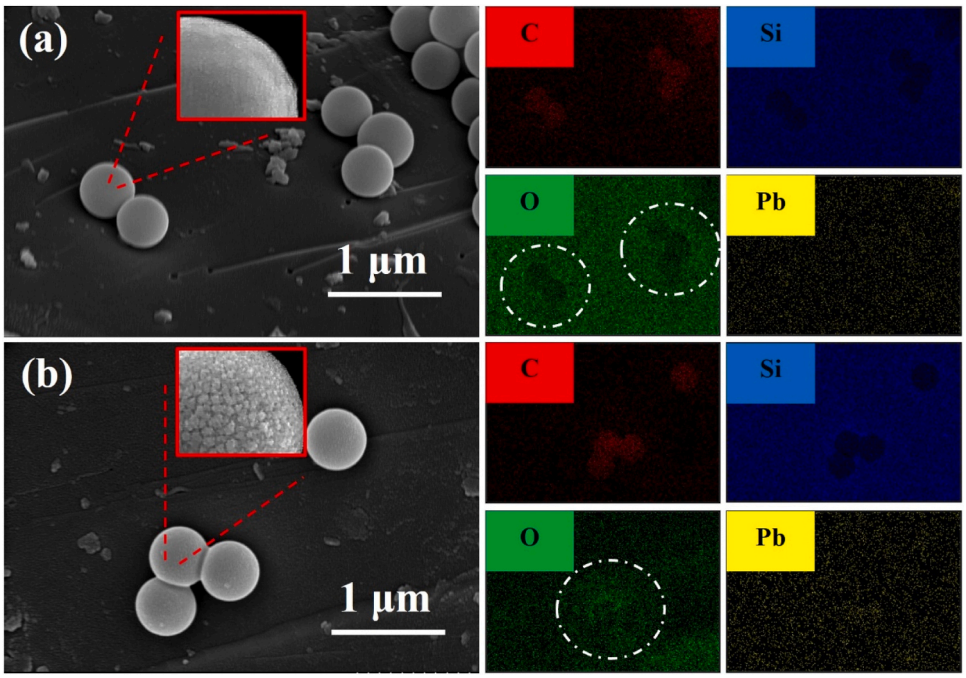

Fig. 1. SEM-Mapping Images: Deposition of MPs/aged MPs and elemental distribution (C, O, Si, Pb) on quartz sand surface.

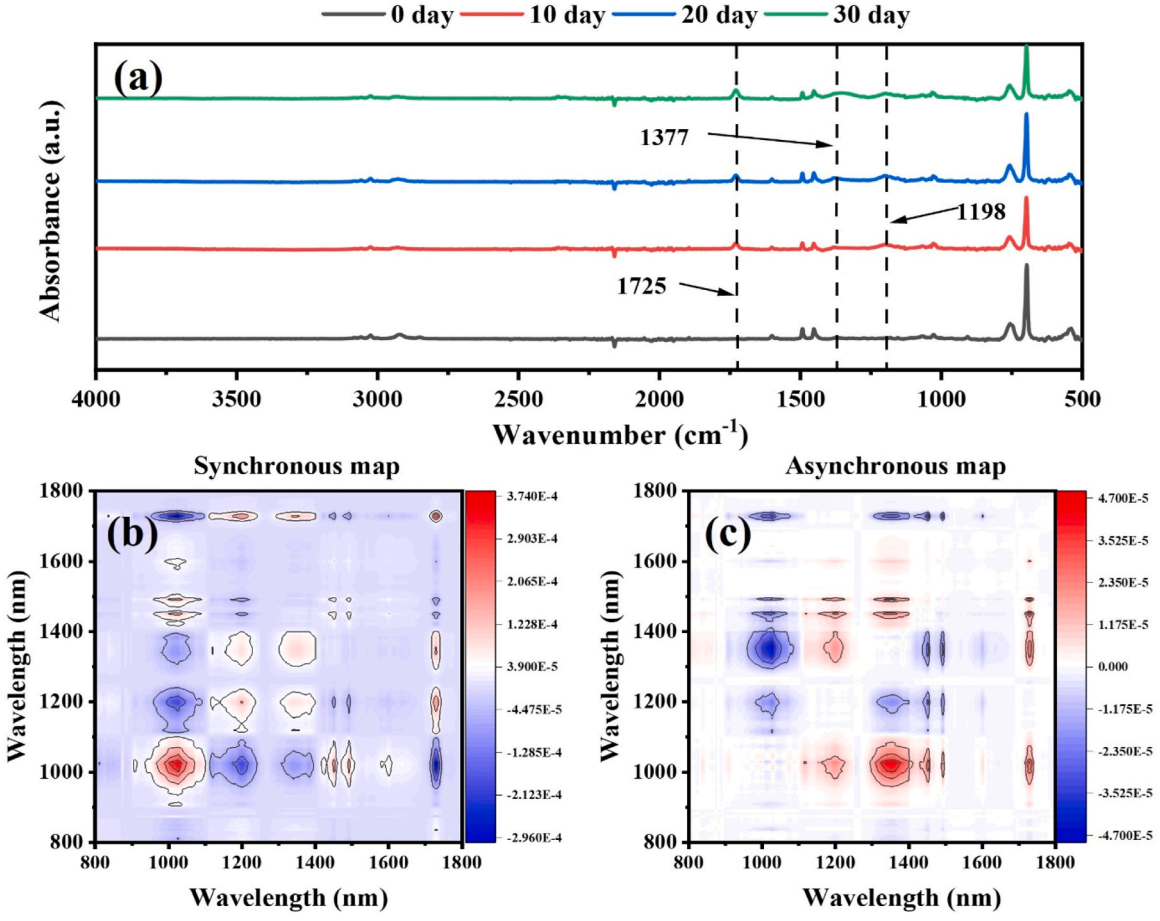

Fig. 2. Fourier spectrograms (a) and 2D-COS correlation maps (Synchronous (b) and Asynchronous (c)) of MPs exposed to different durations of UV irradiation, including 30 days.

compared to pristine MPs.

The FTIR results show changes in the surface functional groups of MPs before and after aging (Fig. 2). For the original functional groups of MPs, the absorption peak at 3000–3100 cm^{-1} is attributed to the stretching vibration of benzene ring C−H bonds [50], while the peaks at 2926 cm^{-1} and 2848 cm^{-1} correspond to the asymmetric and symmetric stretching vibrations of $-CH_2$ groups [18], respectively. The peaks at 1599 cm^{-1} , 1493 cm^{-1} , and 1456 cm^{-1} are associated with the deformation and skeletal vibrations of $-CH_2$ groups [9], and the peak at 1028 cm^{-1} represents the C−H bond of benzene ring cleavage [34]. In addition, UV irradiation leads to the formation of new oxygen-containing functional groups on the surface of aged MPs. For example, the characteristic peak of the C−OH bond in phenol appears at 1377 cm^{-1} , and peaks at 1725 cm^{-1} (O−C═O and C═O stretching), and 1198 cm^{-1} (C−O−C) were observed [25,34]. The oxygen content can be used to indicate the degree of aging in MPs. XPS characterization analysis was performed on MPs before and after aging, which showed an increase in surface oxygen content from 4.46% to 21.67% after UV irradiation (Fig. 3).

To further elucidate the sequence of changes in various functional groups during the 30-day aging process and the mechanism of MPs aging, a 2D-COS analysis was performed based on one-dimensional FTIR spectral data (Fig. 2). Six autocorrelation peaks were observed at 1028, 1198, 1377, 1456, 1493, and 1725 cm^{-1} along the synchronous map diagonal. The intensity ranking of these free peaks is as follows: 1456, 1493, 1377, 1198, 1725, and 1028 cm^{-1} in descending order. This sequence highlights that the most notable alteration appears within the 1725/1028 cm^{-1} band. The asynchrony map, characterized by diagonal antisymmetry, portrays only the asynchrony between two wave numbers, resulting in the presence of cross peaks exclusively [8]. According to the Noda rule and the asynchronous correlation spectra, the order of specific chemical reactions during the aging of MPs can be revealed. Based on the 2D-COS analysis of UV-irradiated aged MPs, the order of spectral changes can be deduced as follows: 1456 > 1493 > 1028 > 1198 > 1725 > 1377 (Table S1). The main reason for the increase in oxygen-containing functional groups in aged MPs is probably the cleavage of C−H bonds in the benzene ring during UV irradiation, leading to the formation of peroxyl radicals and the absorption of hydrogen atoms from the surrounding environment to form new oxygen-containing functional groups [58,59]. Thus, in aged samples, C−O and O−H bonds are initially formed, then, as aging progresses, some of these bonds are converted to C═O bonds, and finally, a small fraction is converted to O−C═O bonds and C−OH bonds.

3.2. Pb(II) adsorption by MPs/aged MPs

3.2.1. Adsorption kinetics

To analyze the adsorption performance and mechanisms of MPs and aged MPs for Pb(II), adsorption kinetics experiments were conducted using MPs before and after UV radiation (Fig. 4a, b). The adsorption capacity of MPs for Pb(II) is 24.83 mg/g, while the adsorption capacity of aged MPs for Pb(II) is 69.13 mg/g. Notably, for pristine MPs, the fitting degree of pseudo-first-order kinetics ($R^2 = 0.9958$) exceeded that of pseudo-second-order kinetics ($R^2 = 0.9949$), indicating that the adsorption behaviors of pristine MPs on Pb(II) align more closely with pseudo-first kinetics, suggesting a dominance of physisorption (Table S2). XPS analysis revealed that the surface of MPs is predominantly carbonaceous (Fig. 3), and the zeta potential of MPs in the experimental aqueous environment was negative (Table S3). Thus, primitive MPs adsorb Pb(II) mainly by electrostatic attraction. On the contrary, concerning aged MPs, we noted a superior fit with the pseudo-second-order kinetics model in contrast to the pseudo-first-order kinetics, demonstrating fitting degrees of $R^2 = 0.9745$ and $R^2 = 0.9949$, respectively. This leads us to conclude that the adsorption behavior of aged MPs on Pb(II) is more consistent with the pseudo-second-order kinetics model, suggesting a mechanism driven by both physical and chemical interactions [42]. This is consistent with previous studies [77]. Oxygen-containing functional groups on the surface of aged MPs can complex with heavy metals. This suggests that UV radiation can induce a change in the interactions between MPs' surface and Pb(II) ions.

The adsorption performance of aged and non-aging MPs towards heavy metal is influenced by their surface structural characteristics [46]. The presence of cracks on the surface of aged MPs leads to increased surface roughness, a higher specific surface area, and more exposed adsorption sites, resulting in stronger adsorption capacity for Pb(II) [26]. Additionally, the aging process introduces new oxygen-containing functional groups (such as −OH, C═O, and −COOH), leading to an increased oxygen-to-carbon ratio (O/C) and enhanced hydrophilicity of the aged MPs' surface, contributing to their stronger adsorption capacity for Pb(II).

Although the applications and solutions are still being researched, the utilization of the intraparticle diffusion kinetics model has been extensively employed in the investigation of the adsorption of metal ions onto adsorbents [65]. The control factors of the adsorption process of Pb (II) by MPs and aged MPs were thereby further investigated using the intraparticle diffusion model (Fig. 4c, d) [43]. Based on the fitting results and model parameters, the adsorption process of the MPs/aged

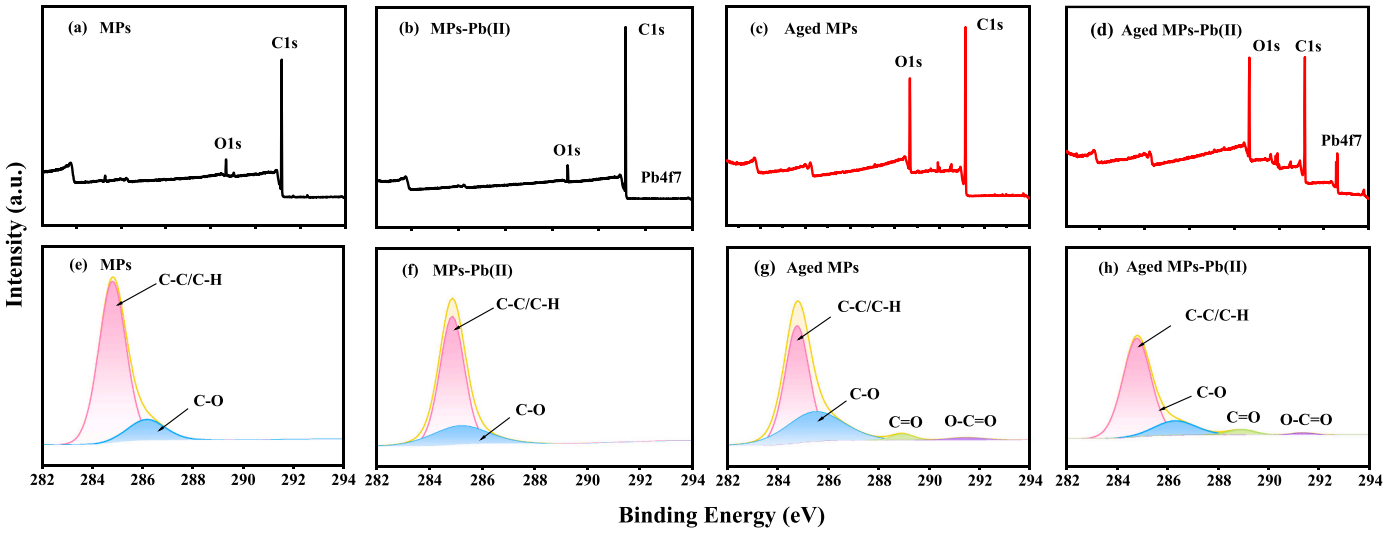

Fig. 3. XPS Spectra of MPs (a), MPs+Pb(II) (b), aged MPs (c), and aged MPs+Pb(II) (d); C1s diagram of MPs(e), MPs+Pb(II) (f), aged MPs (g), and aged MPs+Pb (II) (h).

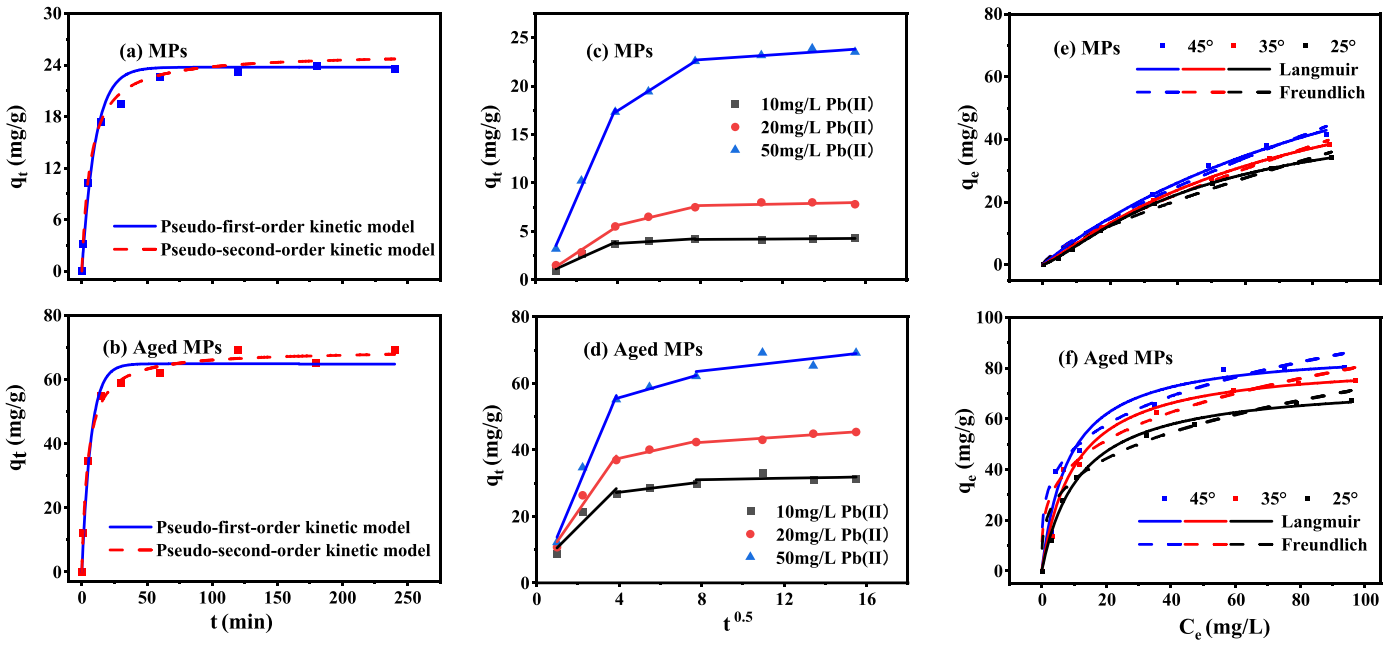

Fig. 4. Fitting of kinetic models for the adsorption of Pb(II) on MPs (a) and aged MPs (b); Fitting of intraparticle diffusion models for the adsorption of Pb(II) on MPs (c) and aged MPs (d); Fitting of isothermal thermodynamic models for the adsorption of Pb(II) on MPs (e) and aged MPs (f).

MPs on Pb(II) can be divided into three stages (0–60 min, 60–240 min, 240–1440 min). In the 0–60 min stage, because the surfaces of MPs and aged MPs have sufficient initial adsorption sites to facilitate the movement of Pb(II) from the solution to the surface to achieve efficient adsorption, the Pb(II) adsorption was predominated by surface diffusion, the adsorption rate of which was extremely high. As the adsorption reaction proceeded, the concentration difference between the solution and the adsorbent was reduced, and some surface adsorption sites of the adsorbent were gradually occupied, resulting in a slower adsorption rate during the 60–240 min stage (Table S4); thus, surface diffusion and intraparticle diffusion became the dominant factors during this stage. In the 240–1440 min stage, the Pb(II) adsorption sites were mostly saturated, and its adsorption and desorption rates were comparable, implying the adsorption-desorption equilibrium was reached.

3.2.2. *Adsorption isotherms and thermodynamics*

Fig. 4e and f demonstrate the adsorption characteristics of MPs and aged MPs on Pb(II) at varying temperatures (25 ℃, 35 ℃, and 45 ℃). The findings revealed an increase in Pb(II) adsorption from 34.29 mg/g to 41.58 mg/g for MPs and from 71.14 mg/g to 93.49 mg/g for aged MPs as temperature rose. This suggests that the adsorption process becomes more favorable at higher temperatures. Furthermore, the Pb(II) adsorption efficiency of aged MPs was found to be superior to that of non-aged MPs. The Langmuir model was found to provide a better fit for the adsorption of Pb(II) by MPs and aged MPs, indicating a monolayer adsorption for Pb(II) at MPs and aged MPs surfaces (Table S5) [44].

Adsorption free energy (ΔG), adsorption enthalpy (ΔH) and adsorption entropy (ΔS) were calculated by ln_{Kd} and the linear fitting of ln_{Kd} and $1/T$ (Table S6) to gain further thermodynamic insights pertaining to Pb(II) adsorption. The negative ΔG values and its increase in absolute values with temperature confirm the spontaneity of the adsorption process and the favorable nature of the process at higher temperatures promoting adsorption [15]. The positive ΔH values indicate that the adsorption process is endothermic, consistent with the findings of the Langmuir model. In summary, the adsorption of Pb(II) by MPs/aged MPs is a spontaneous endothermic process [43].

3.2.3. *XPS analysis of Pb(II) adsorption by MPs and aged MPs*

The XPS spectra disclosed minimal presence of Pb(II) on the surface of pristine MPs, suggesting a weak adsorption capacity for Pb(II) (Fig. 3b). Simultaneously, the C1s spectra of the MPs exhibit only minimal changes. This can be attributed to the weak complexation between the MPs and Pb(II), possibly due to their predominantly carbon composition with a limited presence of oxygen-containing functional groups (Fig. 3f). In contrast, aged MPs exhibited a significant transformation upon Pb(II) adsorption (Figs. 3d and 3h). The XPS spectra displayed the presence of Pb4f7 and a notable increase in oxygen content from 21.67% to 26.2%. The rise in oxygen content implies the formation of surface complexes between aged MPs and Pb(II). It indicates that surface complexation plays a primary role in the adsorption of Pb(II) by aged MPs [19]. It was found that there was no shift at the hydrocarbon-associated peak in the C1s region, but the oxygen-containing functional group shifted. The most notable shift was observed for C−O, which moved from 285.59 eV to 286.38 eV. This indicates that, during the adsorption of Pb(II) onto aged MPs, C−O bonds, which are among the newly formed oxygen-containing functional groups during the aging process, assume a dominant role in facilitating the adsorption and capture of Pb(II).

Specifically, the oxygen atoms on C−O bonds provide lone pairs of electrons capable of forming coordination bonds with Pb(II) [1]. This enables secure bonds to form between Pb(II) and the C−O groups, effectively capturing them. This indicates that, during the adsorption of Pb(II) onto aged MPs, C−O bonds, which are among the newly formed oxygen-containing functional groups during the aging process, assume a dominant role in facilitating the adsorption and capture of Pb(II). This coordination mechanism also stabilizes the position of Pb(II) on the aged MPs' surface. Furthermore, C−O bonds offer supplementary adsorption sites, enabling the physical adsorption of Pb(II) on the aged MPs' surface. This substantially enhances the adsorption capacity of MPs for Pb (II). Additionally, the increase in surface charge density due to the presence of C−O bonds increases the electronegativity of the aged MPs' surfaces, enhancing their electrostatic interaction with charged Pb(II) [70]. Consequently, this charge-based interaction strengthens the adsorption of Pb(II) on the aged MPs' surface. In addition to surface complexation, negatively charged surfaces of aged MPs can engage in electrostatic interactions with positively charged Pb(II). Moreover, the complex and rough surface topography of aged MPs contributes to a higher specific surface area, which correlates with a greater average

saturation adsorption capacity for Pb(II). This implies that van der Waals forces also influence the adsorption behavior between aged MPs and Pb (II) [41].

In summary, the adsorption of Pb(II) by aged MPs involves a complex mechanism including surface complexation, electrostatic interactions, and van der Waals forces. The XPS analysis highlights the crucial role of oxygen-containing functional groups, particularly C−O, in the Pb(II) capture process.

3.3. Mutual influence between MPs/aged MPs and Pb(II) during their co-transport process in homogeneous porous system

In the previous section, the results of batch adsorption experiments indicated that aged MPs are more likely to adsorb Pb(II) with their surface oxygen functional groups. This suggests that, in comparison with Pb(II) transport separately, co-transport with aged MPs is probably broadening the environmental distribution range of Pb(II) owing to the load by aged MPs, which results in more serious synergistic pollution and a greater potential threat to ecosystems. Therefore, it is necessary to investigate the co-transport of MPs/aged MPs and Pb(II), which further elucidates the differences in transport behavior among them.

3.3.1. Influence of MPs and aged MPs on Pb(II) transport

The permeability of Pb(II) through the quartz sand column increased from 50% (IS 1 mM), 62% (IS 10 mM), and 67% (IS 20 mM) to 58%, 65%, and 72% in the presence of MPs, while increasing to 72%, 87%, and 89% in the presence of aged MPs, respectively (Fig. 5). The presence of MPs or aged MPs significantly enhanced the breakthrough capacity of Pb(II) compared to Pb(II) transport alone within quartz sand columns.

The observed phenomenon can be attributed to the differences in Pb (II) transport mechanisms between an independent transport system and a co-transport system. In an independent transport system, the primary mode of Pb(II) transport involves the migration of water-soluble Pb(II) ions alongside the water flow. The presence of quartz sand inevitably hinders Pb(II) transport through electrostatic trapping, as evidenced by changes in the zeta potential value when coexisting with Pb(II) before and after (Table S7). As previously highlighted, both MPs and aged MPs possess the capability to adsorb Pb(II). When Pb(II) coexists with MPs/aged MPs in a water body, a fraction of the Pb(II) becomes adsorbed onto the surface of the MPs/aged MPs. Consequently, co-transport of Pb(II) and MPs occurs, leading to the observation of a heightened peak in the breakthrough curve of Pb(II).

Furthermore, the influence of MPs and aged MPs on the breakthrough ability of Pb(II) exhibits significant disparities. Clearly, aged MPs facilitate the transport of Pb(II) more effectively. In the co-transport system, the mobility of MPs or aged MPs and their adsorption capacity for Pb(II) are the primary factors causing this difference. The experimental results of adsorption indicate that aged MPs possess a stronger adsorption capacity for Pb(II) compared to MPs (Fig. 4). Moreover, the comparison of breakthrough curves clearly illustrates the significantly superior breakthrough capacity of aged MPs over MPs (Fig. 6a, c). It can be deduced logically from the above two aspects that aged MPs can carry a greater amount of Pb(II) in the co-transport process, which is in line with the experimental observations from Fig. 5. Theoretically, the mobility of MPs or aged MPs relates to their stability as well as their interaction forces with quartz sand. The results of aggregation experiments reveal that the homogeneous aggregation phenomenon of pristine MPs was slightly more pronounced than that of aged MPs (Figs. 7a and 7c). Furthermore, sedimentation experiments demonstrate that the sedimentation rate of aged MPs in suspension was significantly slower compared to that of MPs (Figs. 7e and 7g). UV aging induces the formation of new oxygen-containing functional groups on the surface of MPs, leading to an increase in electronegativity (Table S3). According to the classical DLVO theory, this enhanced electronegativity results in improved stability of aged MPs particles [17]. The DLVO calculations also showed that after undergoing UV aging, the repulsive energy barrier between aged MPs and quartz sand increased from 1924 (IS 1 mM), 1388 (IS 10 mM), and 879 kT (IS 20 mM) to 2372 (IS 1 mM), 2021 (IS 10 mM), and 1542 kT (IS 20 mM). UV aging induces a surge in the negative surface charge of aged MPs, substantially amplifying their hydrophilic properties. This change concurrently fortifies the repulsive energy barrier between aged MPs and quartz sand coexisting within the solution milieu, ultimately bolstering the breakthrough capacity of aged MPs. Also, the Hydrus-1D fitting results revealed that the reversible adsorption rate and the irreversible adsorption rate of MPs on quartz sand were both higher than those of aged MPs, indicating a greater tendency for MPs to remain on the quartz sand surface (Table 1). Moreover, ion competition adsorption experiments demonstrated that aged MPs exhibited superior adsorption capabilities for Pb(II) in comparison to non-aging MPs under varying ionic strengths (Fig. S3), implying that even under high background ion concentrations (20 mM), aged MPs can significantly enhance the transport of Pb(II) in saturated porous media.

3.3.2. Effect of Pb(II) on the transport capacity of MPs and aged MPs

The transportability of Pb(II) in porous media is increased by the surface load of MPs/aged MPs, while the coexistence of Pb(II) significantly decreases the permeability of MPs/aged MPs (Fig. 6b, d). Under different background ionic strengths (IS 1, 10, and 20 mM), the breakthrough ability of MPs decreases from 52%, 37%, and 24% to 30%, 23%, and 16%, while the breakthrough ability of aged MPs decreases from 58%, 43%, and 33% to 39%, 34%, and 29%. Previous studies have shown that metal cations can weaken the electrostatic repulsion between particles by neutralizing the negative charge on the particle surface and compressing the double layer of the particles [6,39]. Consequently, it can be inferred that the presence of Pb(II) weakened the electrostatic repulsion between MPs/aged MPs and quartz sand, resulting in the destabilization of MPs/aged MPs particles in suspension. For

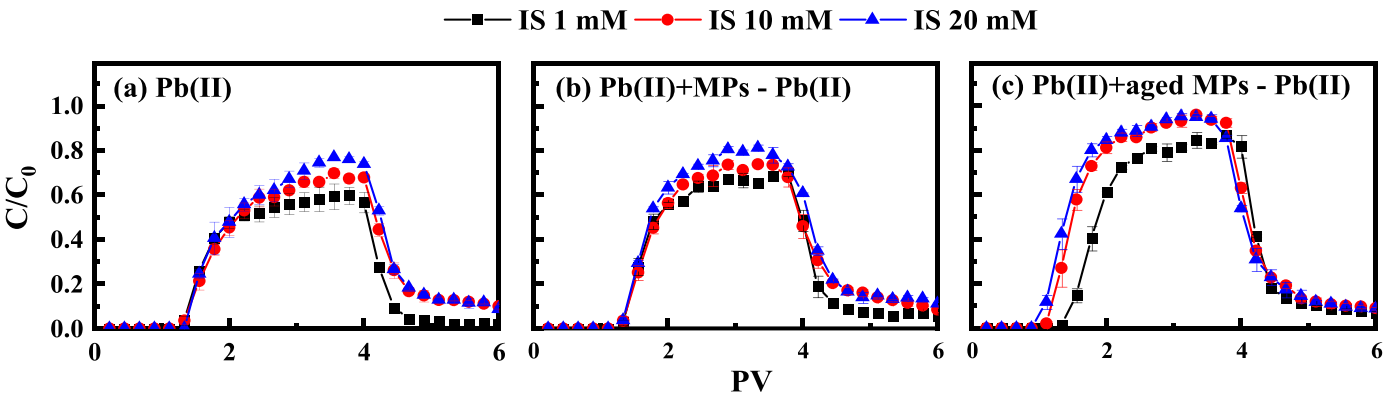

Fig. 5. The breakthrough curve of Pb(II) transport alone (a); co-transport with MPs (b); and co-transport with aged MPs (c) in statured quartz sand column.

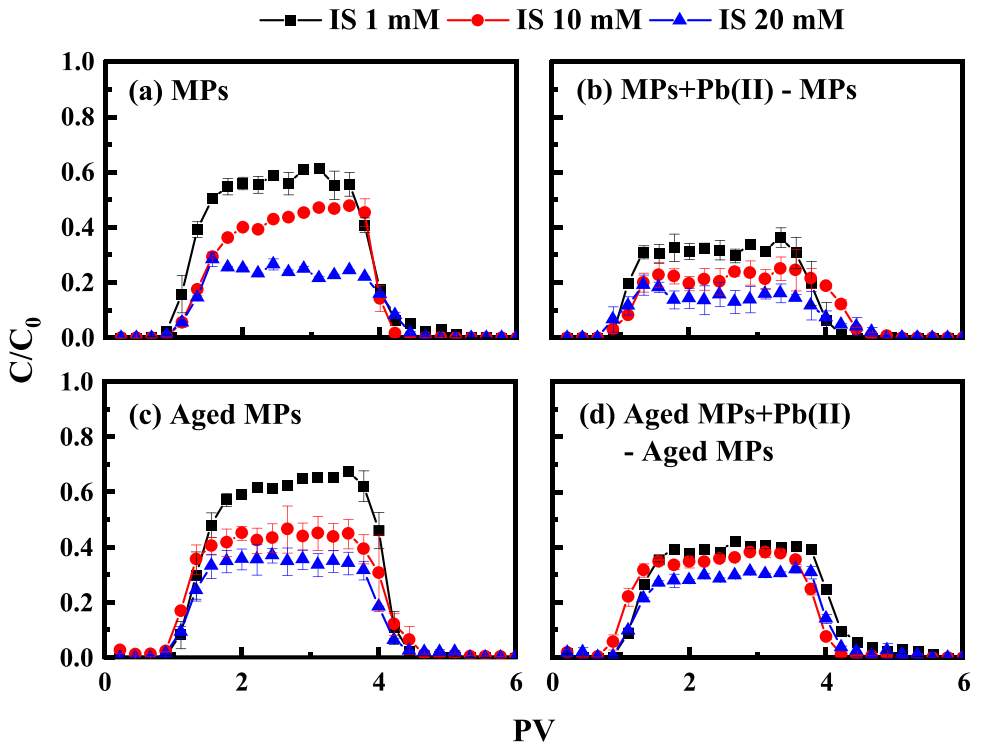

Fig. 6. Breakthrough curves for MPs/aged MPs: MPs transport alone (a); MPs co-transport with Pb(II) (b); aged MPs transport alone (c); and aged MPs co-transport with Pb(II) (d).

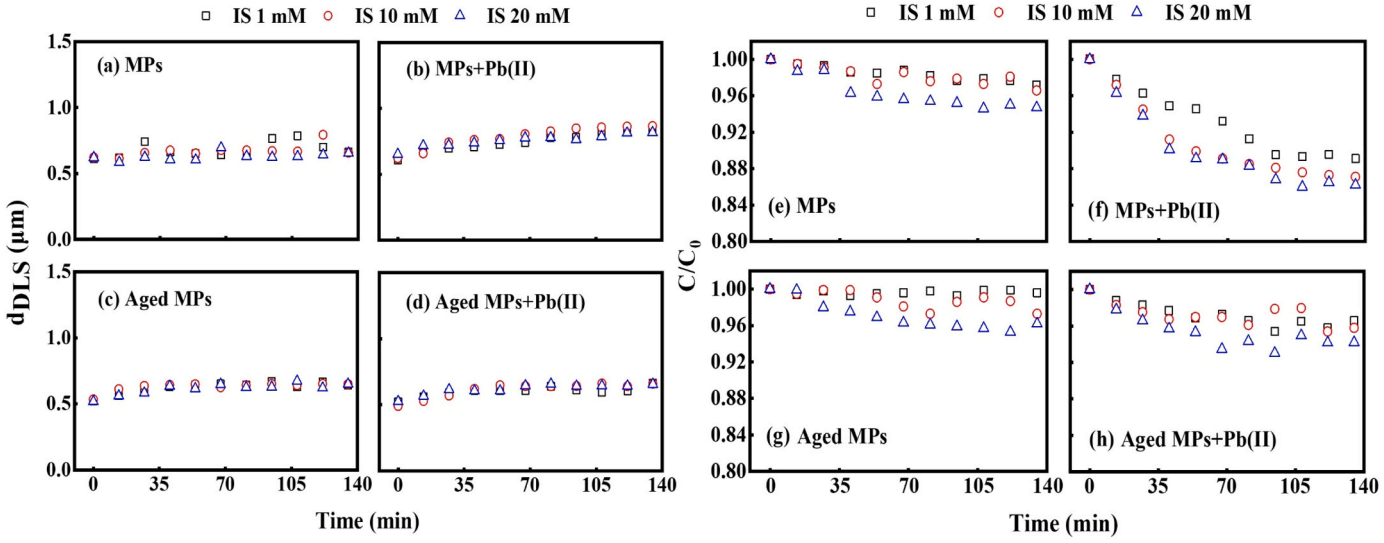

Fig. 7. Aggregation kinetic curves of (a) MPs, (b) MPs+Pb(II), (c) Aged MPs, and (d) Aged MPs+Pb(II) at varying Na^+ ionic strengths; Sedimentation kinetic curves of (e) MPs, (f) MPs+Pb(II), (g) Aged MPs, and (h) Aged MPs+Pb(II) at varying Na^+ ionic strengths.

example, the repulsive energy barrier calculated by DLVO theory between MPs/aged MPs and quartz sand in the presence of Pb(II) was only 777/1358 kT, compared to 1388/2022 kT at a background ion concentration of 10 mM (Fig. 8). The reduced repulsive energy barrier between MPs/aged MPs and quartz sand surfaces in the presence of Pb(II) will unavoidably reduce the ability of MPs/aged MPs to migrate. The sedimentation experimental results (Fig. 7) and two-point kinetic modeling (Table 1) further proved that the sedimentation rate and the adsorption rate of MPs/aged MPs on the quartz sand surface increase significantly in the presence of Pb(II).

In addition, previous research has shown that the bridging effect of divalent metal ions is also an important factor affecting colloid transport [71,74]. Indeed, Pb(II) exhibits the ability to bridge between the particles of MPs/aged MPs as well as between MPs/aged MPs and quartz sand. This bridging effect may have a dual impact: it could promote the aggregation of MPs/aged MPs particles and obstruct the small pores within the quartz sand, facilitating the deposition of MPs/aged MPs [39].

Table 1
The recovery percentages of MPs, aged MPs, and Pb(II) in column experiments, as well as the fitting parameters of the two-point kinetic model.

Fitting objects	Sample	IS (mM)	Recocery (%)	k_1[a] (min-1)	k_{1d}[b]	k_2[c]
MPs	MPs	1	52%	0.93226	0.24465	0.01904
		10	37%	1.52720	0.30063	0.02815
		20	24%	1.94280	0.59135	0.03871
Aged MPs	Aged MPs	1	58%	0.51240	0.36972	0.01150
		10	43%	1.24770	0.51780	0.21695
		20	33%	1.50840	0.61560	0.02837
Pb(II)	Pb(II)	1	50%	2.14920	0.57437	0.14640
		10	62%	1.01610	0.13793	0.11131
		20	67%	0.80315	0.12883	0.00849
MPs	MPs+Pb (II)	1	30%	2.56360	1.08560	0.36626
		10	23%	2.99110	1.12600	0.03741
		20	16%	3.26240	0.44693	0.08012
Aged MPs	Aged MPs+Pb (II)	1	39%	1.15120	0.39361	0.02459
		10	34%	1.41890	0.50542	0.03431
		20	29%	2.02630	0.63506	0.35227
Pb(II)	MPs+Pb (II)	1	58%	1.29260	0.22480	0.13287
		10	65%	0.90916	0.12660	0.01061
		20	72%	0.77667	0.13526	0.00759
	Aged MPs+Pb (II)	1	72%	1.04030	0.20462	0.00649
		10	87%	0.76120	0.14670	0.00336
		20	89%	0.44848	0.10301	0.00280

[a] The first-order attachment rate coefficient on site 1.
[b] The first-order detachment rate coefficient on site 1.
[c] The first-order attachment rate coefficient on site 2.

3.4. Effect of biochar on the transport of aged MPs and Pb(II) in heterogeneous porous system

The aforementioned studies have verified the notable transport efficiency of aged MPs and Pb(II) in a homogeneous porous system under various treatments. However, as described in the introduction, how do the transport properties of two environmental pollutants change in a heterogeneous porous system where biochar and quartz sand coexist? Accordingly, drawing upon methodologies employed in previous studies [62,67], biochar was incorporated into quartz sand to explore the distinct transport characteristics of these two environmental pollutants in a heterogeneous porous system. Following the inclusion of biochar into the quartz sand, the presence of aged MPs in the effluent became nearly non-existent (Fig. 9a). It is evident that almost all of the aged MPs used in the study had deposited within the column and were unable to escape. Upon observing and comparing Figs. 5a and 9b, the recovery of Pb(II) decreased from 50% (IS 1 mM), 62% (IS 10 mM), and 67% (IS 20 mM) to 0% (IS 1 mM), 4% (IS 10 mM), and 5% (IS 20 mM). These experimental findings underscore the substantial inhibitory effect of biochar on the individual transport of both pollutants.

The limited mobility of aged MPs and Pb(II) within the heterogeneous porous system can be rationalized by the excellent adsorption capacity of biochar towards these two contaminants [56,62]. Compared to quartz sand, biochar has a more complex pore structure (7.8935 cm^3/g), larger specific surface area (34.3572 m^2/g), and more oxygen-containing functional groups (Fig. S4), which means that larger amounts of two pollutants will probably be trapped by biochar. This

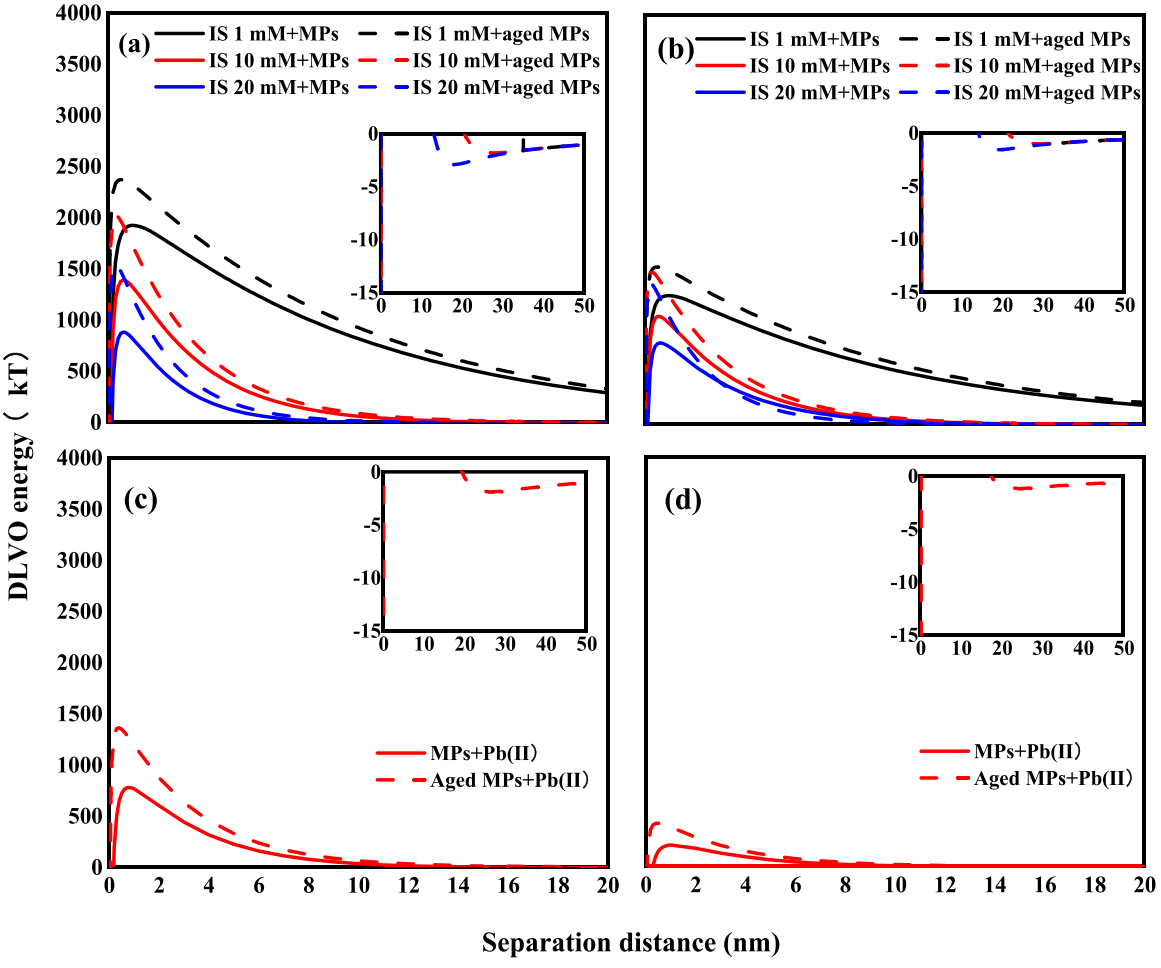

Fig. 8. DLVO interaction energy calculations: MPs/aged MPs with quartz sand (a) and biochar (b) in different background ion concentrations; MPs/aged MPs with quartz sand (c) and biochar (d) in Pb(II) solutions.

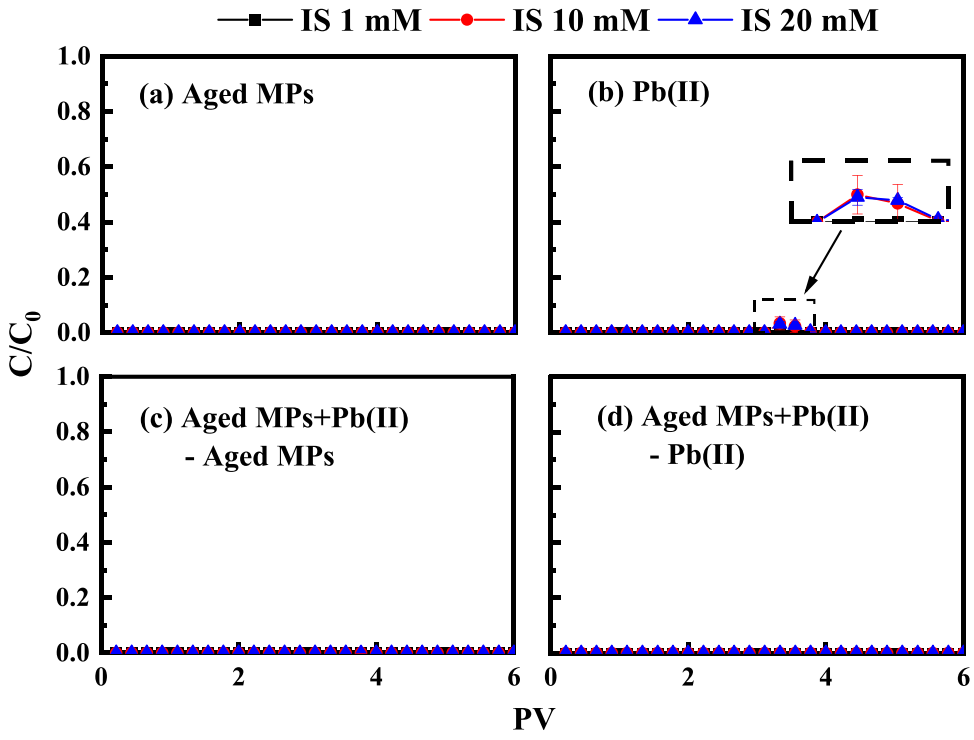

Fig. 9. The breakthrough curve of aged MPs/Pb(II) in quartz sand with biochar as a porous medium: aged MPs transport alone (a); Pb(II) transport alone (b); aged MPs in the co-transport system (c); Pb(II) in the co-transport system (d).

argument can be backed up by the following two aspects: On the one hand, the results of the composite adsorption experiments demonstrated that the addition of biochar to quartz sand further heightened the adsorption efficiency for Pb(II) (Fig. S6). Existing research indicates that key adsorption mechanisms for heavy metals onto biochar encompass physical adsorption, ion exchange, electrostatic adsorption, precipitation, complexation, and reduction [22]. The efficacy of biochar in heavy metal adsorption primarily hinges on factors such as its specific surface area and the abundance of surface-active functional groups [57]. The intricate structure of biochar offers numerous adsorption sites, while its surface's oxygen-containing functional groups readily form complexes with heavy metal ions [54,57]. This results in a significant inhibition of Pb(II) transport. On the other hand, the DLVO energies depicted in Fig. 8 showed that there is a lower repulsive energy barrier between aged MPs and biochar compared to the one between aged MPs and quartz sand. It shows in theory that the stronger bond between aged MPs and biochar makes it easier for the MPs to settle into biochar-containing heterogeneous porous media. Previous studies have suggested that biochar, with a relatively complex surface morphology and irregular shape, could bind MPs more tightly [24]. In addition, despite the fact that the biochar was small enough to be uniformly distributed in the pores of the column, the porosity and pore volume of the column did not change, implying that the plugging effect may not be the dominant mechanism for inhibiting the transport of aged MPs [16]. In conclusion, the robust adsorption capacity of biochar plays a pivotal role in inhibiting the transport of both pollutants. This underscores the practical significance of biochar in mitigating the migration of environmental contaminants, providing a promising avenue for environmental remediation.

In addition to the aforementioned findings, an intriguing observation came to light. Traditionally, colloids have been considered carriers that facilitate the transport of heavy metals through saturated porous media [19,37]. In this study, when Pb(II) was allowed to transport through heterogeneous porous medium independently, a small fraction of Pb(II) was detectable in the effluent (as shown in the inserted figure in Fig. 9b). However, when aged MPs and Pb(II) were co-transported within a biochar-included sand column, the Pb(II) in the effluent was nearly undetectable, indicating a more pronounced inhibition of Pb(II) transport. SEM-mapped images of Fig. S5 also revealed substantial quantities of MPs particles and Pb(II) on the surface and within the cracks of the biochar following the transport experiments. The transport capacity of Pb(II) is closely tied to the mobility of its carriers, specifically aged MPs, as previously discussed. The inclusion of biochar in the quartz sand matrix significantly affected the mobility of aged MPs particles. Aged MPs are incapable of permeating through the heterogeneous porous media. Consequently, a fraction of the Pb(II) absorbed by the aged MPs co-deposits with them within the media, resulting in the suppression of Pb(II)' penetration ability. These findings are supported by the experimental results of the composite adsorption experiments. When quartz sand, biochar, and aged MPs collectively adsorbed Pb(II), there was virtually no detectable Pb(II) remaining in the solution (Fig. S6). Essentially, the introduction of biochar not only hampers the individual mobility of aged MPs but also contributes to the co-deposition of Pb(II) alongside aged MPs within the column, ultimately suppressing the overall mobility of Pb(II). These findings not only enhance our comprehension of colloid-mediated contaminant transport but also underscore the potential applications of biochar in immobilizing plastic particles and heavy metals. Further research into the underlying mechanisms and the optimization of biochar application in remediating contaminated soil offer promising avenues for environmental management and sustainable development.

4. Conclusion

In this study, the adsorption of Pb(II) by UV-aged MPs and their co-transport in saturated homogeneous and heterogeneous porous media were explored, leading to the following key conclusions:

Firstly, when pristine MPs are exposed to UV light, significant physicochemical changes occur, such as the formation of new oxygen-containing functional groups, a decrease in surface electronegativity, and an increase in surface roughness and specific surface area, enhancing their adsorptive and migration capacity to Pb(II) in a homogeneous medium. Secondly, the investigation revealed that biochar-

included heterogeneous media effectively hinder the co-transport of aged MPs and Pb(II). This hindrance is primarily attributed to the inherently poor mobility of MPs, leading to the co-deposition of the adsorbed portion of heavy metals with MPs. Consequently, this co-deposition phenomenon significantly diminishes the migration capacity of lead ions. The distinctive properties of biochar, particularly its highly porous structure and functional groups, play a pivotal role in facilitating the joint capture and immobilization of both aged MPs and Pb(II).

Overall, this study provides nuanced insights into the complex interactions between UV-aged MPs, Pb(II), and biochar in both homogeneous and heterogeneous porous media, offering valuable perspectives on effective strategies for curtailing the environmental mobility of MPs and heavy metals.

Environmental implication

Our research extensively investigates the co-transport behavior of UV-aged MPs and Pb(II) in porous media, specifically within two migration systems: quartz sand and quartz sand with added biochar as a porous medium. UV-aged MPs, with their heightened Pb(II) adsorption capacity, have the potential to introduce composite pollutants, posing risks to both human health and ecosystems. Our work elucidates critical interaction mechanisms between MPs, aged MPs, and Pb(II) within these porous media systems, offering essential insights into their transport dynamics. This understanding is instrumental in devising effective strategies for controlling and mitigating the spread of these pollutants, thereby contributing to environmental protection. The use of biochar as a porous medium further demonstrates its potential to inhibit pollutant transport.

CRediT authorship contribution statement

Chang Bokun: Conceptualization, Data curation, Formal analysis, Validation, Writing – original draft. **Xu Chenyang:** Project administration. **Hu Feinan:** Investigation, Validation. **Yang Yajun:** Investigation, Validation. **Cao Gang:** Investigation, Resources. **Ding Wei:** Formal analysis, Methodology. **Zhong Xianbao:** Data curation, Validation. **Fang Xianhui:** Data curation, Investigation. **Yang Tianhuan:** Data curation, Investigation, Resources. **Du Wei:** Funding acquisition, Resources, Supervision, Writing – review & editing. **Yang Xiaodong:** Formal analysis, Investigation, Methodology. **Lv Jialong:** Funding acquisition, Project administration, Resources, Supervision, Writing – review & editing. **Huang Zixuan:** Data curation, Methodology. **Qiu Ling:** Investigation, Methodology.

Declaration of Competing Interest

The authors declare that they have no known competing financial interests or personal relationships that could have appeared to influence the work reported in this paper.

Data Availability

Data will be made available on request.

Acknowledgements

This work was supported by the National Natural Science Foundation of China (Nos. 42077135 and 42107332), the Natural Science Basic Research Program of Shaanxi Province, China (No. 2021JQ-170), the Agricultural Science and Technology Innovation Plan of Shaanxi Province, China (NYKJ-2022-YL(XN)39), and the Agricultural Key-scientific and Core-technological Project of Shaanxi Province (2023NYGG011).

Appendix A. Supporting information

Supplementary data associated with this article can be found in the online version at doi:10.1016/j.jhazmat.2023.133413.

References

[1] Ahmad, S.Z.N., Wan Salleh, W.N., Ismail, A.F., Yusof, N., Mohd Yusop, M.Z., Aziz, F., 2020. Adsorptive removal of heavy metal ions using graphene-based nanomaterials: toxicity, roles of functional groups and mechanisms. Chemosphere 248, 126008.
[2] Alimi, O.S., Farner Budarz, J., Hernandez, L.M., Tufenkji, N., 2018. Microplastics and nanoplastics in aquatic environments: aggregation, deposition, and enhanced contaminant transport. Environ Sci Technol 52 (4), 1704–1724.
[3] Atugoda, T., Vithanage, M., Wijesekara, H., Bolan, N., Sarmah, A.K., Bank, M.S., et al., 2021. Interactions between microplastics, pharmaceuticals and personal care products: implications for vector transport. Environ Int 149, 106367.
[4] Bradford, S.A., Simunek, J., Bettahar, M., van Genuchten, M.T., Yates, S.R., 2003. Modeling colloid attachment, straining, and exclusion in saturated porous media. Environ Sci Technol 37 (10), 2242–2250.
[5] Brennecke, D., Duarte, B., Paiva, F., Caçador, I., Canning-Clode, J., 2016. Microplastics as vector for heavy metal contamination from the marine environment. Estuar, Coast Shelf Sci 178, 189–195.
[6] Cao, G., Sun, J., Chen, M., Sun, H., Zhang, G., 2021. Co-transport of ball-milled biochar and Cd^{2+} in saturated porous media. J Hazard Mater 416.
[7] Chang, B., He, B., Cao, G., Zhou, Z., Liu, X., Yang, Y., et al., 2023. Co-transport of polystyrene microplastics and kaolinite colloids in goethite-coated quartz sand: joint effects of heteropolymerization and surface charge modification. Sci Total Environ 884, 163832.
[8] Chen, W., Teng, C.-Y., Qian, C., Yu, H.-Q., 2019. Characterizing properties and environmental behaviors of dissolved organic matter using two-dimensional correlation spectroscopic analysis. Environ Sci Technol 53 (9), 4683–4694.
[9] Chia, C.H., Gong, B., Joseph, S.D., Marjo, C.E., Munroe, P., Rich, A.M., 2012. Imaging of mineral-enriched biochar by FTIR, Raman and SEM–EDX. Vib Spectrosc 62, 248–257.
[10] Collin, M.S., Venkatraman, S.K., Vijayakumar, N., Kanimozhi, V., Arbaaz, S.M., Stacey, R.G.S., et al., 2022. Bioaccumulation of lead (Pb) and its effects on human: a review. J Hazard Mater Adv 7.
[11] Collin, S., Baskar, A., Geevarghese, D.M., Ali, M.N.V.S., Bahubali, P., Choudhary, R., et al., 2022. Bioaccumulation of lead (Pb) and its effects in plants: a review. J Hazard Mater Lett 3.
[12] De Bhowmick, G., Sarmah, A.K., 2022. Microplastics contamination associated with land-application of biosolids: a perspective. Curr Opin Environ Sci Health 26.
[13] Derjaguin, B., Landau, L., 1993. Theory of the stability of strongly charged lyophobic sols and of the adhesion of strongly charged particles in solutions of electrolytes. Prog Surf Sci 43 (1-4), 30–59.
[14] Ding, T., Wei, L., Hou, Z., Li, J., Zhang, C., Lin, D., 2022. Microplastics altered contaminant behavior and toxicity in natural waters. J Hazard Mater 425, 127908.
[15] Ding, W., Liang, H., Zhang, H., Sun, H., Geng, Z., Xu, C., 2023. A cellulose/bentonite grafted polyacrylic acid hydrogel for highly-efficient removal of Cd(II). J Water Process Eng 51.
[16] Dong, Z., Qiu, Y., Zhang, W., Yang, Z., Wei, L., 2018. Size-dependent transport and retention of micron-sized plastic spheres in natural sand saturated with seawater. Water Res 143, 518–526.
[17] Dong, Z., Zhang, W., Qiu, Y., Yang, Z., Wang, J., Zhang, Y., 2019. Cotransport of nanoplastics (NPs) with fullerene (C60) in saturated sand: effect of NPs/C60 ratio and seawater salinity. Water Res 148, 469–478.
[18] Fang, S., Yu, W., Li, C., Liu, Y., Qiu, J., Kong, F., 2019. Adsorption behavior of three triazole fungicides on polystyrene microplastics. Sci Total Environ 691, 1119–1126.
[19] Fu, Q., Tan, X., Ye, S., Ma, L., Gu, Y., Zhang, P., et al., 2021. Mechanism analysis of heavy metal lead captured by natural-aged microplastics. Chemosphere 270, 128624.
[20] Gong, H., Zhao, L., Rui, X., Hu, J., Zhu, N., 2022. A review of pristine and modified biochar immobilizing typical heavy metals in soil: applications and challenges. J Hazard Mater 432, 128668.
[21] Gregory, J., 1981. Approximate expressions for retarded van der waals interaction. J Colloid Interface Sci 83 (1), 138–145.
[22] Gupta, S., Sireesha, S., Sreedhar, I., Patel, C.M., Anitha, K., 2020. Latest trends in heavy metal removal from wastewater by biochar based sorbents. J Water Process Eng 38, 101561.
[23] Hsieh, L., He, L., Zhang, M., Lv, W., Yang, K., Tong, M., 2022. Addition of biochar as thin preamble layer into sand filtration columns could improve the microplastics removal from water. Water Res 221, 118783.
[24] Hsieh, L., He, L., Zhang, M., Lv, W., Yang, K., Tong, M., 2022. Addition of biochar as thin preamble layer into sand filtration columns could improve the microplastics removal from water. Water Res 221, 118783.
[25] Huffer, T., Weniger, A.K., Hofmann, T., 2018. Sorption of organic compounds by aged polystyrene microplastic particles. Environ Pollut 236, 218–225.
[26] Jiang, Y., Qin, Z., Fei, J., Ding, D., Sun, H., Wang, J., et al., 2022. Surfactant-induced adsorption of Pb(II) on the cracked structure of microplastics. J Colloid Interface Sci 621, 91–100.

[27] Jiang, Y., Yin, X., Xi, X., Guan, D., Sun, H., Wang, N., 2021. Effect of surfactants on the transport of polyethylene and polypropylene microplastics in porous media. Water Res 196, 117016.
[28] Jin, T., Tang, J., Lyu, H., Wang, L., Gillmore, A.B., Schaeffer, S.M., 2022. Activities of microplastics (MPs) in agricultural soil: a review of MPs pollution from the perspective of agricultural ecosystems. J Agric Food Chem 70 (14), 4182–4201.
[29] Kah, M., Sigmund, G., Xiao, F., Hofmann, T., 2017. Sorption of ionizable and ionic organic compounds to biochar, activated carbon and other carbonaceous materials. Water Res 124, 673–692.
[30] Khalid, N., Aqeel, M., Noman, A., Khan, S.M., Akhter, N., 2021. Interactions and effects of microplastics with heavy metals in aquatic and terrestrial environments. Environ Pollut 290, 118104.
[31] Kim, T., Park, K., Hong, J., 2022. Understanding the hazards induced by microplastics in different environmental conditions. J Hazard Mater 424 (Pt C), 127630.
[32] Koelmans, A.A., Bakir, A., Burton, G.A., Janssen, C.R., 2016. Microplastic as a vector for chemicals in the aquatic environment: critical review and model-supported reinterpretation of empirical studies. Environ Sci Technol 50 (7), 3315–3326.
[33] Koelmans, A.A., Redondo-Hasselerharm, P.E., Nor, N.H.M., de Ruijter, V.N., Mintenig, S.M., Kooi, M., 2022. Risk assessment of microplastic particles. Nat Rev Mater 7 (2), 138–152.
[34] Lang, M., Yu, X., Liu, J., Xia, T., Wang, T., Jia, H., et al., 2020. Fenton aging significantly affects the heavy metal adsorption capacity of polystyrene microplastics. Sci Total Environ 722.
[35] Li, J., Song, Y., Cai, Y., 2020. Focus topics on microplastics in soil: analytical methods, occurrence, transport, and ecological risks. Environ Pollut 257, 113570.
[36] Li, M., He, L., Zhang, M., Liu, X., Tong, M., Kim, H., 2019. Cotransport and deposition of iron oxides with different-sized plastic particles in saturated quartz sand. Environ Sci Technol 53 (7), 3547–3557.
[37] Li, M., He, L., Zhang, X., Rong, H., Tong, M., 2020. Different surface charged plastic particles have different cotransport behaviors with kaolinite particles in porous media. Environ Pollut 267, 115534.
[38] Li, S., Liang, C., Shangguan, Z., 2017. Effects of apple branch biochar on soil C mineralization and nutrient cycling under two levels of N. Sci Total Environ 607 109–119.
[39] Li, X., Xu, H., Gao, B., Yang, Z., Sun, Y., Shi, X., et al., 2019. Cotransport of Herbaspirillum chlorophenolicum FA1 and heavy metals in saturated porous media: effect of ion type and concentration. Environ Pollut 254 (Pt A), 112940.
[40] Li, Y., Yu, H., Liu, L., Yu, H., 2021. Application of co-pyrolysis biochar for the adsorption and immobilization of heavy metals in contaminated environmental substrates. J Hazard Mater 420, 126655.
[41] Li, Y., Zhang, Y., Su, F., Wang, Y., Peng, L., Liu, D., 2022. Adsorption behaviour of microplastics on the heavy metal Cr(VI) before and after ageing. Chemosphere 302, 134865.
[42] Liang, H., Ding, W., Zhang, H., Peng, P., Peng, F., Geng, Z., et al., 2022. A novel lignin-based hierarchical porous carbon for efficient and selective removal of Cr (VI) from wastewater. Int J Biol Macromol 204, 310–320.
[43] Liang, H., Sun, R., Song, B., Sun, Q., Peng, P., She, D., 2020. Preparation of nitrogen-doped porous carbon material by a hydrothermal-activation two-step method and its high-efficiency adsorption of Cr(VI). J Hazard Mater 387.
[44] Liang, H., Zhang, H., Zhao, P., Zhao, X., Sun, H., Geng, Z., et al., 2021. Synthesis of a novel three-dimensional porous carbon material and its highly selective Cr(VI) removal in wastewater. J Clean Prod 306.
[45] Ling, X., Yan, Z., Liu, Y., Lu, G., 2021. Transport of nanoparticles in porous media and its effects on the co-existing pollutants. Environ Pollut 283, 117098.
[46] Liu, S., Huang, J., Zhang, W., Shi, L., Yi, K., Yu, H., et al., 2022. Microplastics as a vehicle of heavy metals in aquatic environments: a review of adsorption factors, mechanisms, and biological effects. J Environ Manag 302 (Pt A), 113995.
[47] Liu, S., Shi, J., Wang, J., Dai, Y., Li, H., Li, J., et al., 2021. Interactions between microplastics and heavy metals in aquatic environments: a review. Front Microbiol 12, 652520.
[48] Liu, Z., Zhu, Y., Lv, S., Shi, Y., Dong, S., Yan, D., et al., 2021. Quantifying the dynamics of polystyrene microplastics UV-aging process. Environ Sci Technol Lett 9 (1), 50–56.
[49] Luo, Z., Zhou, X., Su, Y., Wang, H., Yu, R., Zhou, S., et al., 2021. Environmental occurrence, fate, impact, and potential solution of tire microplastics: similarities and differences with tire wear particles. Sci Total Environ 795, 148902.
[50] Ma, J., Zhao, J., Zhu, Z., Li, L., Yu, F., 2019. Effect of microplastic size on the adsorption behavior and mechanism of triclosan on polyvinyl chloride. Environ Pollut 254 (Pt B), 113104.
[51] Mao, R., Lang, M., Yu, X., Wu, R., Yang, X., Guo, X., 2020. Aging mechanism of microplastics with UV irradiation and its effects on the adsorption of heavy metals. J Hazard Mater 393, 122515.
[52] Marquardt, D.W., 1963. An algorithm for least-squares estimation of nonlinear parameters. J Soc Ind Appl Math 11 (2), 431–441.
[53] Nguyen, T.B., Ho, T.B., Huang, C.P., Chen, C.W., Chen, W.H., Hsieh, S., et al., 2022. Adsorption of lead(II) onto PE microplastics as a function of particle size: influencing factors and adsorption mechanism. Chemosphere 304, 135276.
[54] Ni, B.-J., Huang, Q.-S., Wang, C., Ni, T.-Y., Sun, J., Wei, W., 2019. Competitive adsorption of heavy metals in aqueous solution onto biochar derived from anaerobically digested sludge. Chemosphere 219, 351–357.
[55] Oladoja, N.A., Unuabonah, I.E., 2021. The pathways of microplastics contamination in raw and drinking water. J Water Process Eng 41.
[56] Qian, L., Zhang, W., Yan, J., Han, L., Gao, W., Liu, R., et al., 2016. Effective removal of heavy metal by biochar colloids under different pyrolysis temperatures. Bioresour Technol 206, 217–224.
[57] Qiu, B., Tao, X., Wang, H., Li, W., Ding, X., Chu, H., 2021. Biochar as a low-cost adsorbent for aqueous heavy metal removal: A review. J Anal Appl Pyrolysis 155, 105081.
[58] Ren, Z., Gui, X., Wei, Y., Chen, X., Xu, X., Zhao, L., et al., 2021. Chemical and photo-initiated aging enhances transport risk of microplastics in saturated soils: Key factors, mechanisms, and modeling. Water Res 202, 117407.
[59] Ren, Z., Gui, X., Xu, X., Zhao, L., Qiu, H., Cao, X., 2021. Microplastics in the soil-groundwater environment: Aging, migration, and co-transport of contaminants - a critical review. J Hazard Mater 419, 126455.
[60] Shen, Y., 2015. Chars as carbonaceous adsorbents/catalysts for tar elimination during biomass pyrolysis or gasification. Renew Sustain Energy Rev 43, 281–295.
[61] Tang, S., Lin, L., Wang, X., Feng, A., Yu, A., 2020. Pb(II) uptake onto nylon microplastics: Interaction mechanism and adsorption performance. J Hazard Mater 386, 121960.
[62] Tong, M., He, L., Rong, H., Li, M., Kim, H., 2020. Transport behaviors of plastic particles in saturated quartz sand without and with biochar/Fe3O4-biochar amendment. Water Res 169, 115284.
[63] Tripathi, M., Sahu, J.N., Ganesan, P., 2016. Effect of process parameters on production of biochar from biomass waste through pyrolysis: a review. Renew Sustain Energy Rev 55, 467–481.
[64] Verwey, E.J., Overbeek, J.T., 1947. Theory of the stability of lyophobic colloids. J Colloid Sci.
[65] Wang, J., Guo, X., 2022. Rethinking of the intraparticle diffusion adsorption kinetics model: interpretation, solving methods and applications. Chemosphere 309 (Pt 2), 136732.
[66] Wang, Q., Duan, C.-j, Xu, C.-y, Geng, Z.-c, 2022. Efficient removal of Cd (II) by phosphate-modified biochars derived from apple tree branches: processes, mechanisms, and application. Sci Total Environ 819, 152876.
[67] Wang, X., Dan, Y., Diao, Y., Liu, F., Wang, H., Sang, W., 2022. Transport and retention of microplastics in saturated porous media with peanut shell biochar (PSB) and MgO-PSB amendment: co-effects of cations and humic acid. Environ Pollut 305, 119307.
[68] Wang, Z., Luo, P., Zha, X., Xu, C., Kang, S., Zhou, M., et al., 2022. Overview assessment of risk evaluation and treatment technologies for heavy metal pollution of water and soil. J Clean Prod 379.
[69] Wright, S.L., Kelly, F.J., 2017. Plastic and human health: a micro issue? Environ Sci Technol 51 (12), 6634–6647.
[70] Xi, X., Ding, D., Zhou, H., Baihetiyaer, B., Sun, H., Cai, Y., et al., 2022. Interactions of pristine and aged nanoplastics with heavy metals: Enhanced adsorption and transport in saturated porous media. J Hazard Mater 437.
[71] Xia, T., Lin, Y., Li, S., Yan, N., Xie, Y., He, M., et al., 2021. Co-transport of negatively charged nanoparticles in saturated porous media: Impacts of hydrophobicity and surface O-functional groups. J Hazard Mater 409, 124477.
[72] Xiang, Y., Jiang, L., Zhou, Y., Luo, Z., Zhi, D., Yang, J., et al., 2022. Microplastics and environmental pollutants: Key interaction and toxicology in aquatic and soil environments. J Hazard Mater 422, 126843.
[73] Yang, Y., Yuan, W., Hou, J., You, Z., 2022. Review on physical and chemical factors affecting fines migration in porous media. Water Res 214, 118172.
[74] Yao, J., Wang, H., Ma, C., Cao, Y., Chen, W., Gu, L., et al., 2022. Cotransport of thallium(I) with polystyrene plastic particles in water-saturated porous media. J Hazard Mater 422, 126910.
[75] Zhang, K., Hamidian, A.H., Tubic, A., Zhang, Y., Fang, J.K.H., Wu, C., et al., 2021. Understanding plastic degradation and microplastic formation in the environment: a review. Environ Pollut 274, 116554.
[76] Zhou, D., Cai, Y., Yang, Z., 2022. Key factors controlling transport of micro- and nanoplastic in porous media and its effect on coexisting pollutants. Environ Pollut 293, 118503.
[77] Zhou, Z., Sun, Y., Wang, Y., Yu, F., Ma, J., 2022. Adsorption behavior of Cu (II) and Cr (VI) on aged microplastics in antibiotics-heavy metals coexisting system. Chemosphere 291, 132794.